

The intermediate-age open clusters Ruprecht 61, Czernik 32, NGC 2225 and NGC 2262

G. Carraro^{1,2} \star , G. Baume³, R.A. Vázquez³, A. Moitinho⁴, and D. Geisler⁵

¹*Departamento de Astronomía, Universidad de Chile, Casilla 36-D, Santiago, Chile*

²*Astronomy Department, Yale University, P.O. Box 208101, New Haven, CT 06520-8101, USA*

³*Facultad de Ciencias Astronómicas y Geofísicas de la UNLP, IALP-CONICET, Paseo del Bosque s/n, La Plata, Argentina*

⁴*CAAUL, Observatório Astronómico de Lisboa, Tapada da Ajuda, 1349-018 Lisboa, Portugal*

⁵*Universidad de Concepción, Departamento de Física, Casilla 160-C, Concepción, Chile*

Submitted: February 2005

ABSTRACT

We present the first *BVI* CCD photometry to $V = 22.0$ of 4 fields centered on the region of the southern Galactic star clusters Ruprecht 61, Czernik 32, NGC 2225 and NGC 2262 and of 4 displaced control fields. These clusters were never studied before, and we provide for the first time estimates of their fundamental parameters, namely radial extent, age, distance and reddening. We find that the four clusters are all of intermediate age (around 1 Gyr), close to the Sun and possess lower than solar metal abundance.

Key words: Open clusters and associations: general – open clusters and associations: individual: Ruprecht 61, Czernik 32, NGC 2225, NGC 2262

1 INTRODUCTION

This paper continues a series dedicated to the study of open clusters in the third Galactic Quadrant, and aims at addressing fundamental questions like the structure of the spiral arms in this quadrant, and the precise definition of the Galactic disk radial abundance gradient outside the solar circle. A more detailed illustration of the motivations of this project are given in Moitinho (2001) and Baume et al (2004). Here we concentrate on four intermediate-age clusters (about the age of the Hyades - 600 Myrs - or older) Ruprecht 61 (VdB-Hagen 32), Czernik 32 (VdB-Hagen 11), NGC 2225 and NGC 2262, for which we provide the first photometric data and try to clarify their nature and to derive estimates of their fundamental parameters.

In Table 1 we list the cluster coordinates, which we re-determined from Digital Sky Survey (DSS) maps on a visual inspection basis.

The layout of the paper is as follows. Sect. 2 illustrates the observation and reduction strategies. An analysis of the geometrical structure and star counts in the field of the clusters is presented in Sect. 3, whereas a discussion of the Color-Magnitude Diagrams (CMDs) is performed in Sect. 4.

\star On leave from Dipartimento di Astronomia, Università di Padova, Vicolo Osservatorio 2, I-35122, Padova, Italy. email: gcarraro@das.uchile.cl

Table 1. Basic parameters of the clusters under investigation. Coordinates are for J2000.0 equinox

Name	<i>RA</i>	<i>DEC</i>	<i>l</i>	<i>b</i>
	<i>hh : mm : ss</i>	$^{\circ} : ' : ''$	[deg]	[deg]
Ruprecht 61	08:25:14	-34:08:31	253.48	+2.08
Czernik 32	07:50:30	-29:50:36	245.86	-1.74
NGC 2225	06:26:37	-09:38:07	218.78	-9.86
NGC 2262	06:39:39	+01:08:30	210.57	-2.10

Sect. 5 deals with the determination of clusters' reddening, distance, metallicity and age and, finally, Sect. 6 summarizes our findings.

2 OBSERVATIONS AND DATA REDUCTION

CCD *BVI* observations were carried out with the CCD camera on-board the 1.0m telescope at Cerro Tololo Inter-American Observatory (CTIO, Chile), on the nights of December 13 and 15, 2004. With a pixel size of $0''.469$, and a CCD size of 512×512 pixels, each pointing samples a $4'.1 \times 4'.1$ field on the sky.

The details of the observations are listed in Table 2 where the observed fields are reported together with the exposure times, the average seeing values and the range of air-masses during the observations. Figs. 1 to 4 show I=600 secs images

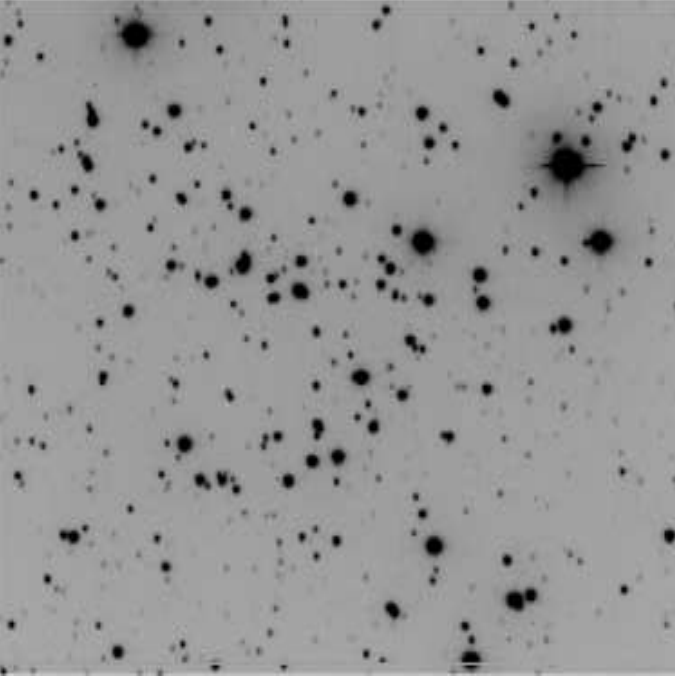


Figure 1. Deep I image (600 secs) of the open cluster Ruprecht 61. North is up, East on the left, and the covered area is $4'.1 \times 4'.1$

obtained in the area of Ruprecht 61, Czernik 32, NGC 2225 and NGC 2262, respectively. Together with the clusters, we observed three control fields 15 arcmins apart from the nominal cluster centers to deal with field star contamination. Exposure of 600 secs in V and I were secured for these fields.

The data have been reduced with the IRAF[†] packages CCDRED, DAOPHOT, ALLSTAR and PHOTCAL using the point spread function (PSF) method (Stetson 1987). The two nights turned out to be photometric and very stable, and therefore we derived calibration equations for all the 130 standard stars observed during the two nights in the Landolt (1992) fields SA 95-41, PG 0231+051, Rubin 149, Rubin 152, T phe and SA 98-670 (see Table 2 for details). The adopted calibration equations are of the form:

$$\begin{aligned} b &= B + b_1 + b_2 \times X + b_3 \times (B - V) \\ v &= V + v_1 + v_2 \times X + v_3 \times (B - V) \\ v &= V + v_{1,i} + v_{2,i} \times X + v_{3,i} \times (V - I) \\ i &= I + i_1 + i_2 \times X + i_3 \times (V - I) , \end{aligned}$$

where BVI are standard magnitudes, bvi are the instrumental ones and X is the airmass; all the coefficient values are reported in Table 3. The standard stars in these fields provide the color coverage $-0.6 \leq (B - V) \leq 2.2$). The final *r.m.s.* of the calibration are 0.031, 0.024 and 0.023 for the B, V and I filters, respectively. We generally used the third equation to calibrate the V magnitude in order to get the same magnitude depth both in the cluster and in the field. Photometric errors have been estimated following closely Patat &

[†] IRAF is distributed by NOAO, which are operated by AURA under cooperative agreement with the NSF.

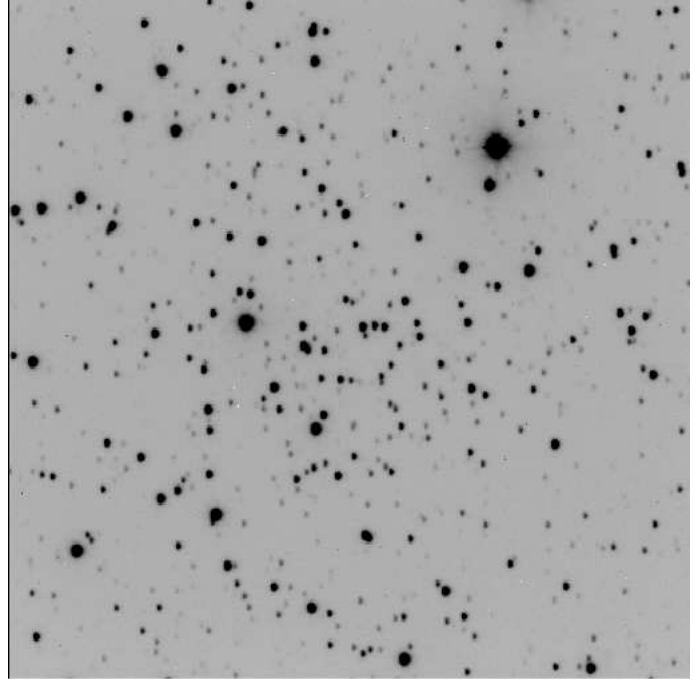


Figure 2. Deep I image (600 secs) of the open cluster Czernik 32. North is up, East on the left, and the covered area is $4'.0 \times 4'.1$

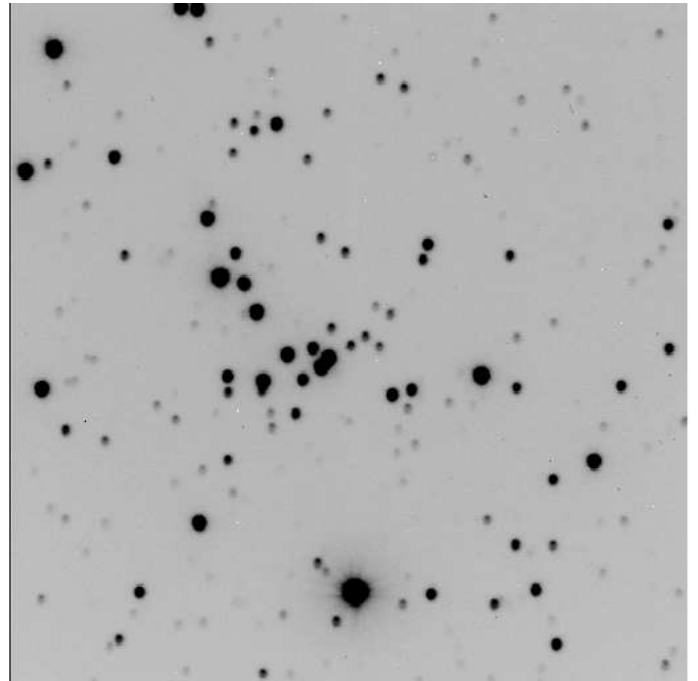


Figure 3. Deep I image (600 secs) of the open cluster NGC 2225. North is up, East on the left, and the covered area is $4'.1 \times 4'.1$

Carraro (2001, Appendix A), which the reader is referred to for all the details. It turns out that the global photometric errors amount to 0.03, 0.05 and 0.20 at $V = 12, 16$ and 21.5 mag, respectively.

The final photometric catalogs for Ruprecht 61, Czernik 32, NGC 2225 and NGC 2262 (coordinates, B, V and I magnitudes and errors) consist of 1166, 1047, 869 and 925 stars,

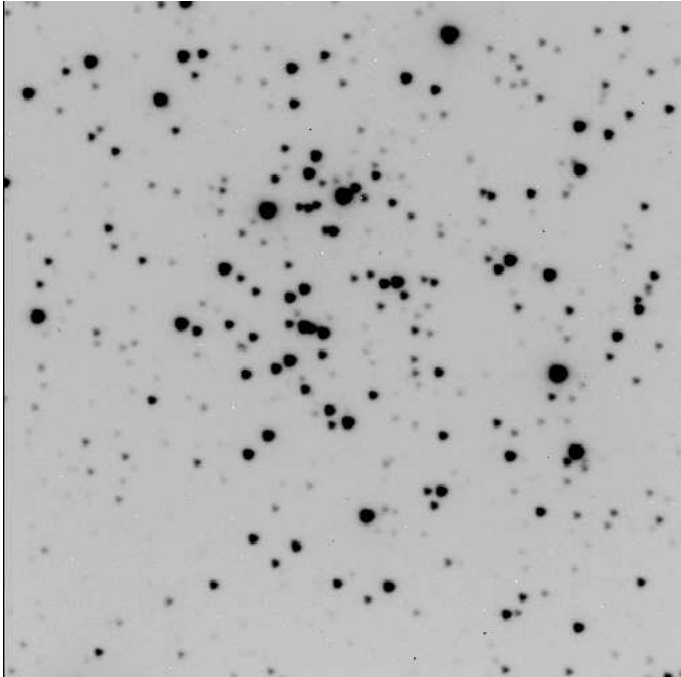


Figure 4. Deep I image (600 secs) of the open cluster NGC 2262. North is up, East on the left, and the covered area is $4'.1 \times 4'.1$

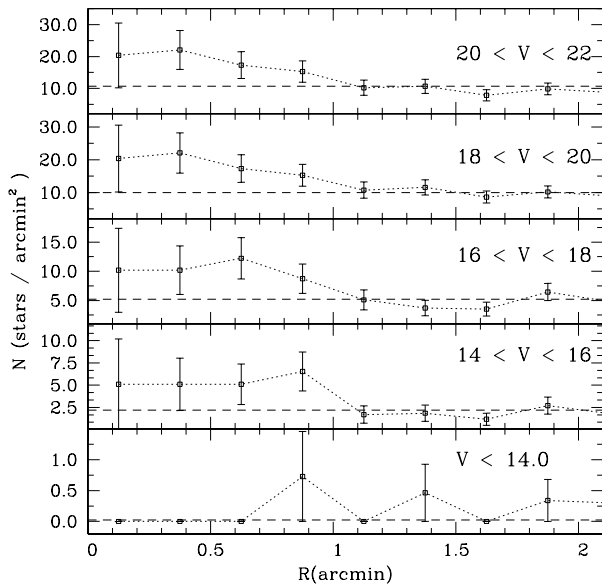


Figure 5. Star counts in the area of Ruprecht 61 as a function of radius and magnitude. The dashed lines represent the level of the control field counts estimated from the accompanying control field.

respectively, and are made available in electronic form at the WEBDA[‡] site maintained by J.-C. Mermilliod.

[‡] <http://obswww.unige.ch/webda/navigation.html>

Table 2. Journal of observations of Ruprecht 61, Pismis 7 and Czernik 32 and standard star fields (December 13 and 15, 2004).

Field	Filter	Exposure time [sec.]	Seeing [\prime]	Airmass
Ruprecht 61	B	120,1200	1.2	1.00-1.10
	V	30,600	1.3	1.00-1.10
	I	30,600	1.2	1.00-1.10
NGC 2262	B	120,1200	1.2	1.15-1.30
	V	30,600	1.3	1.15-1.30
	I	30,600	1.2	1.15-1.30
NGC 2225	B	120,1200	1.2	1.15-1.30
	V	30,600	1.3	1.15-1.30
	I	30,600	1.2	1.15-1.30
Czernik 32	B	120,1200	1.2	1.25-1.40
	V	30,600	1.3	1.25-1.40
	I	30,600	1.2	1.25-1.40
SA 98-670	B	3×120	1.2	1.24-1.26
	V	3×40	1.4	1.24-1.26
	I	3×20	1.4	1.24-1.26
PG 0231+051	B	3×120	1.2	1.20-2.04
	V	3×40	1.5	1.20-2.04
	I	3×20	1.5	1.20-2.04
T Phe	B	3×120	1.2	1.04-1.34
	V	3×40	1.3	1.04-1.34
	I	3×20	1.3	1.04-1.34
Rubin 152	B	3×120	1.3	1.33-1.80
	V	3×40	1.2	1.33-1.80
	I	3×20	1.2	1.33-1.80
Rubin 149	B	3×120	1.1	1.21-1.96
	V	3×40	1.2	1.21-1.96
	I	3×20	1.2	1.21-1.96
SA 95-41	B	3×120	1.2	1.05-1.48
	V	3×40	1.2	1.05-1.48
	I	3×20	1.1	1.05-1.48

Table 3. Coefficients of the calibration equations

$b_1 = 3.465 \pm 0.009$	$b_2 = 0.25 \pm 0.02$	$b_3 = -0.145 \pm 0.008$
$v_1 = 3.244 \pm 0.005$	$v_2 = 0.16 \pm 0.02$	$v_3 = 0.021 \pm 0.005$
$v_{1,i} = 3.244 \pm 0.005$	$v_{2,i} = 0.16 \pm 0.02$	$v_{3,i} = 0.009 \pm 0.005$
$i_1 = 4.097 \pm 0.005$	$i_2 = 0.08 \pm 0.02$	$i_3 = 0.006 \pm 0.005$

3 STAR COUNTS AND CLUSTERS' SIZES

As we will show in this Section, our photometry covers entirely each cluster's area allowing us to perform star counts to obtain improved estimates of the clusters' size. In fact these clusters are generally very faint, poorly populated and compact (see Fig. 1 to 4) and therefore could well fit within the CCD area.

We derived the surface stellar density by performing star counts in concentric rings around the clusters' nominal centers (see Table 1) and then dividing by their respective areas. Poisson errors have also been derived and normalized to the corresponding area. The field star contribution has been de-

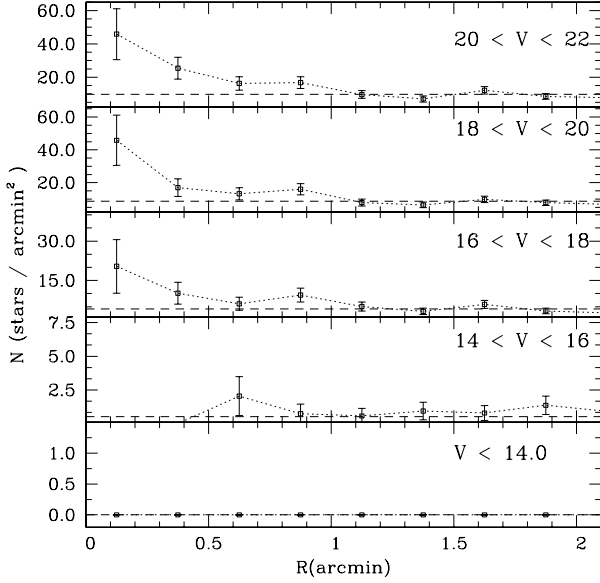


Figure 6. Star counts in the area of Czernik 32 as a function of radius and magnitude. The dashed lines represent the level of the control field counts estimated from the accompanying control field.

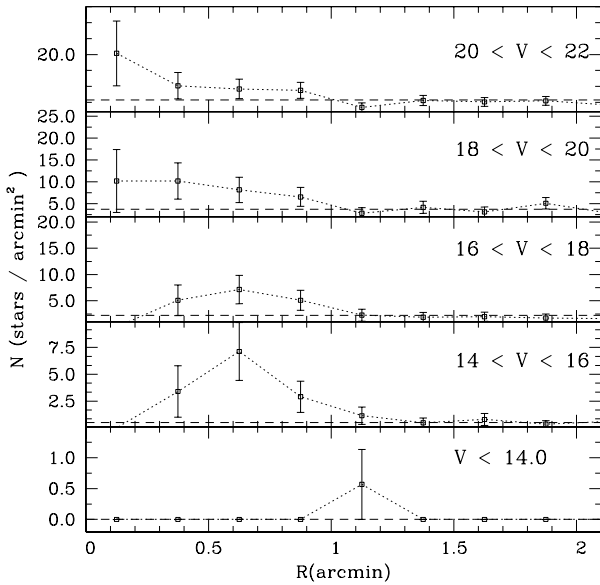


Figure 7. Star counts in the area of NGC 2225 as a function of radius and magnitude. The dashed lines represent the level of the control field counts estimated from the accompanying control field.

rived from the control field which we secured for each cluster, and the errors have been computed in the same way as for the cluster field.

Ruprecht 61 The radial density profile for Ruprecht 61 is shown in Fig. 5 as a function of the V magnitude. Clearly,

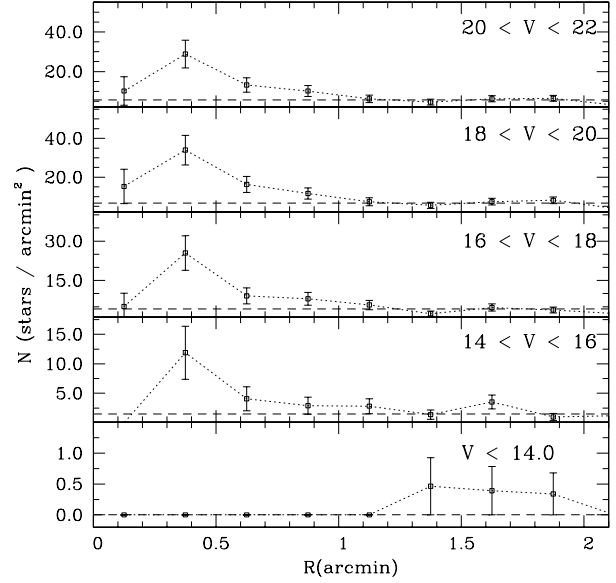


Figure 8. Star counts in the area of NGC 2262 as a function of radius and magnitude. The dashed lines represent the level of the control field counts estimated from the accompanying control field.

the cluster does not appear very concentrated, and it is deficient of bright stars. The cluster seems to emerge from the background in the magnitude range $16 \leq V \leq 22$. In this magnitude range the radius is not larger than 1.0 arcmin. We shall adopt the value of 1.0 arcmin as the radius of Ruprecht 61 throughout this paper. This estimate is in perfect agreement the value of 2.0 arcmin reported by Dias et al. (2002) for the cluster diameter.

Czernik 32 The radial density profile for Czernik 32 is shown in Fig. 6 as a function of the V magnitude. The cluster shows a clear lack of bright stars and it is mostly populated by stars of magnitude in the range $18 \leq V \leq 22$. In this magnitude range the radius is not larger than 1.0 arcmin. In conclusion, we are going to adopt the value of 1.0 arcmin as the Czernik 32 radius throughout this paper. This estimate is in reasonable agreement with the value of 3.0 arcmin reported by Dias et al. (2002) for the cluster diameter.

NGC 2225 The radial density profile for NGC 2225 is shown in Fig. 7 as a function of the V magnitude. Also this cluster exhibits a deficiency of bright stars and it is mostly populated by stars of magnitude in the range $16 \leq V \leq 22$. In this magnitude range the radius is not larger than 1.2 arcmin.

This estimate is in reasonable agreement with (a bit smaller than) the value of 4.0 arcmin reported by Dias et al. (2002) for the cluster diameter.

NGC 2262 The radial density profile for NGC 2262 is shown in Fig. 8 as a function of the V magnitude. This cluster is composed mainly by stars of magnitude in the range $16 \leq V \leq 22$, where the radius is around 1.0 arcmin. In conclusion, we are going to adopt the value of 1.0 arcmin as the

radius of NGC 2262 throughout this paper. This estimate is much smaller than the value of 5.0 arcmin reported by Dias et al. (2002) for the cluster diameter.

The estimates we provide for the radius, although reasonable, must be taken as preliminary. In fact, the size of the CCD is probably too small to derive conclusive estimates of the cluster sizes, that due to dynamical evolution and mass segregation tend to be normally under-estimated. Larger and deep field coverage is necessary to derive firmer estimates of the clusters radii.

4 THE COLOUR-MAGNITUDE DIAGRAMS

In Fig. 9 we present the CMDs obtained for the observed fields of the four clusters under investigation. All the stars observed in each field have been plotted (not only those within the derived cluster radii). In this figure, the open cluster Ruprecht 61 is shown together with the corresponding control field in the lower panels, Czernik 32 and NGC 2225 are presented in the middle panels, while finally NGC 2262 is presented in the upper panels. The control fields help us to better interpret these CMDs, which are clearly affected by strong foreground star contamination.

Ruprecht 61. This cluster is presented in the lower panels of Fig. 9. It exhibits a Main Sequence (MS) extending from $V=15-15.5$, where the Turn Off Point (TO) is located, down to $V=21.5$. This MS is significantly wide, wider than photometric error at a given magnitude (see Sect. 2). We ascribe this to field star contamination, and to the presence of a sizeable binary star population, which mainly enlarge the MS toward red colors. However, the reality of this cluster seems to be secured by the shape of the MS with respect to the control field MS, whose population sharply decreases at $V = 17$. Also, the cluster MS is significantly bluer and more tilted than the field MS, which derives from the superposition of stars of different reddening located at all distances between the cluster and the Sun. Another interesting evidence is the possible presence of a clump of stars at $V=14.5$, which does not have a clear counterpart in the field, and which implies a cluster of intermediate-age. In fact if we use the age calibration from Carraro & Chiosi (2004), for a ΔV (the magnitude difference between the red clump and the TO) of 0.5 mag, we infer an age around 1 Gyr. This estimate does not take into account the cluster metallicity, and therefore is simply a guess. In the following Sect. we shall provide a more robust estimate of the age through a detailed comparison with theoretical isochrones.

Czernik 32. The open cluster Czernik 32 is presented in the lower-mid panels of Fig. 9. The TO located at $V \approx 17$, and a prominent clump at $V \approx 16$ with no counterpart in the field CMD are readily seen, yielding an estimated age of around 1.0 Gyr. The overall morphology of the CMDs is in this case very different from the field CMD leaving no doubt that Czernik 32 is a bona-fide intermediate-age open cluster.

NGC 2225. The open cluster NGC 2225 is presented in the upper-mid panels of Fig. 9. Again, the overall morphology

of the cluster CMDs, with a TO and an evident red clump, is very different from the field CMD. Indeed, the field sequence is much less populated and stops at $V \approx 16.5$, giving a first impression that this is a bona-fide intermediate-age open cluster. The TO located at $V \approx 16$, and red clump at $V \approx 15$, allow to estimate an age of around 1.0 billion years, confirming the first impression that NGC 2225 is an intermediate age cluster.

NGC 2262. The open cluster NGC 2262 is presented in the upper panels of Fig. 9. The cluster's CMD reveals a TO is located at $V \approx 16$, and a possible clump at $V \approx 16$ as well, which provide a rough estimate of around 0.5 Gyrs for the age of NGC 2262. The overall morphology of the CMDs is also in this case very different from the field CMD confirming that this is a bona-fide intermediate-age open cluster.

5 DERIVING CLUSTERS' FUNDAMENTAL PARAMETERS

In this section we are going to perform a detailed comparison of the star distribution in the clusters' CMDs with theoretical isochrones. For this study, we adopt in this study the Padova library from Girardi et al. (2000). This comparison is clearly not an easy exercise. In fact, the detailed shape and position of the various features in the CMD (MS, TO and clump basically) depends mostly on age and metallicity, and then also on reddening and distance. The complex interplay between the various parameters is however well known, and we refer to Chiosi et al. (1992) and Carraro (2005) as nice examples of the underlying technique.

Our basic strategy is to survey different age and metallicity isochrones in an attempt to provide the best fit of all the CMD features both in the V vs $(B - V)$ and in the V vs $(V - I)$ CMD.

To further facilitate the fitting procedure, by increasing the contrast between the cluster and the field population, we shall consider only the stars which lie within the cluster radius as derived in Sect. 3.

Finally, to derive the clusters' distances from reddening and apparent distance modulus, a reddening law must be specified. In this study we shall adopt the normal reddening law $A_v = 3.1 \times E(B - V)$ in deriving the clusters' distances.

Additionally to finding the best fit, we also estimated the uncertainties in the basic parameters. These uncertainties simply reflect the range of parameters that yields a reasonable fit to the clusters CMDs. The errors are reported in Table 4, and an example of the procedure is shown in Fig.10 for the case of Ruprecht 61. The best fit for all the clusters, achieved simultaneously in the V vs $(B - V)$ and in the V vs $(V - I)$ planes, are shown in Figs. 11-14.

Ruprecht 61. The fitting procedure and the isochrone solution for this cluster are shown in Figs. 10 and 11. We obtained the best fit for an age of 1.3 Gyrs and a metallicity $Z=0.008$ (see middle panel of Fig. 11, and Fig. 12). In fact, the shape of the TO in the left panel of Fig. 11 (for the $Z=0.004$ isochrone) is clearly different from the underlying cluster sequence, and the same can be noticed for the $Z=0.019$ isochrone (right panel), where the red hook shows

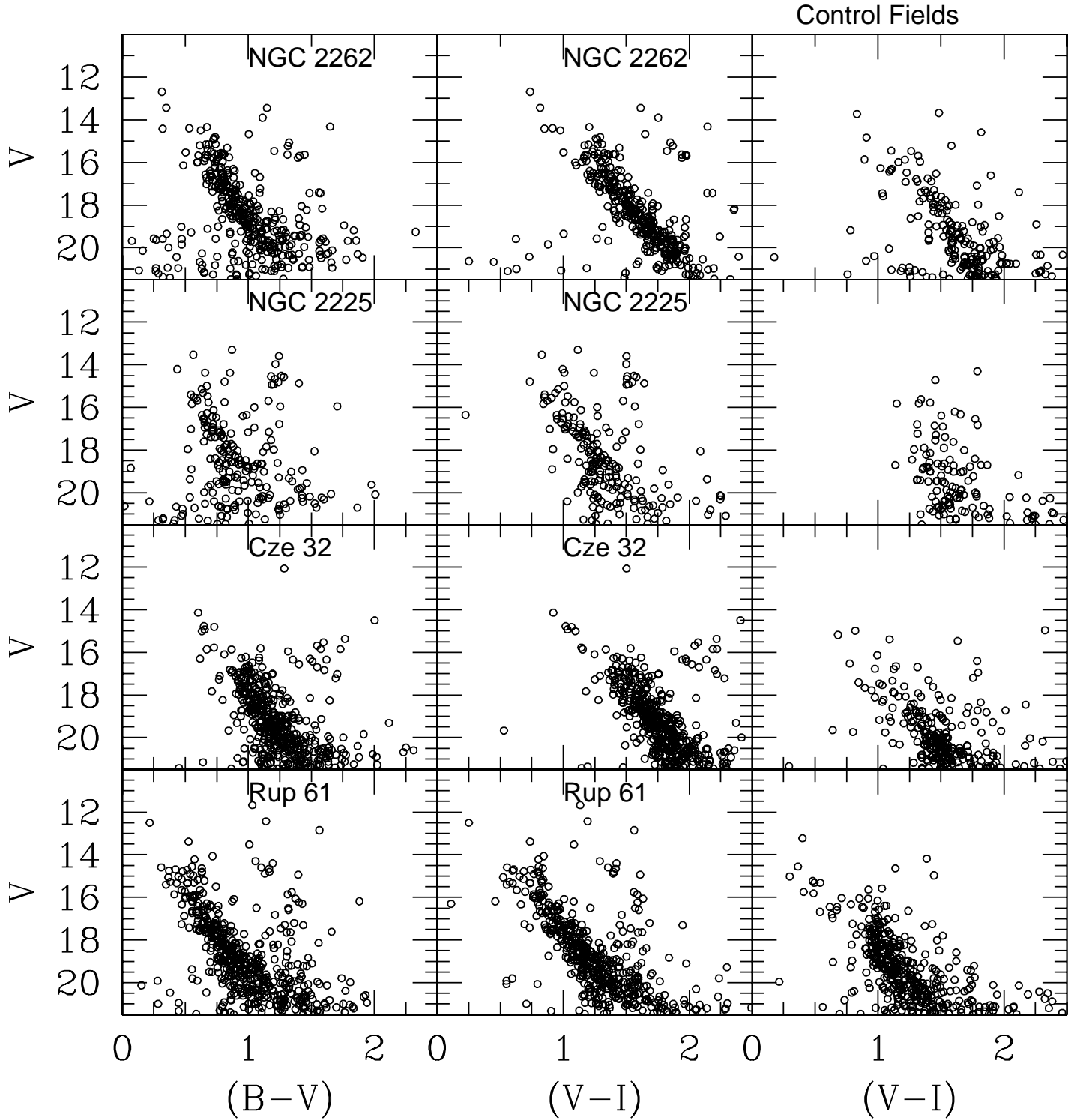


Figure 9. V vs $(B - V)$ (left panels) and V vs $(V - I)$ (middle panels) CMDs of Ruprecht 61, Czernik 32, NGC 2225 and NGC 2262 and corresponding control fields (right panels). We include all stars in each field.

a shape which does not fit very well the star distribution in the cluster. In details, the red hook is too red and somewhat faint with respect to the $Z=0.008$ isochrone and the actual stars distribution. To get a bluer and brighter red hook, one should use a younger isochrone, which will however possess

a too red clump and RGB, when fixed to the TO.

The inferred reddening and apparent distance modulus are $E(B-V)=0.30$ ($E(V-I)=0.41$, right panel in Fig. 12) and $(m-M)=13.85$, respectively. As a consequence, the cluster possesses a heliocentric distance of 3.9 kpc, and is located at a

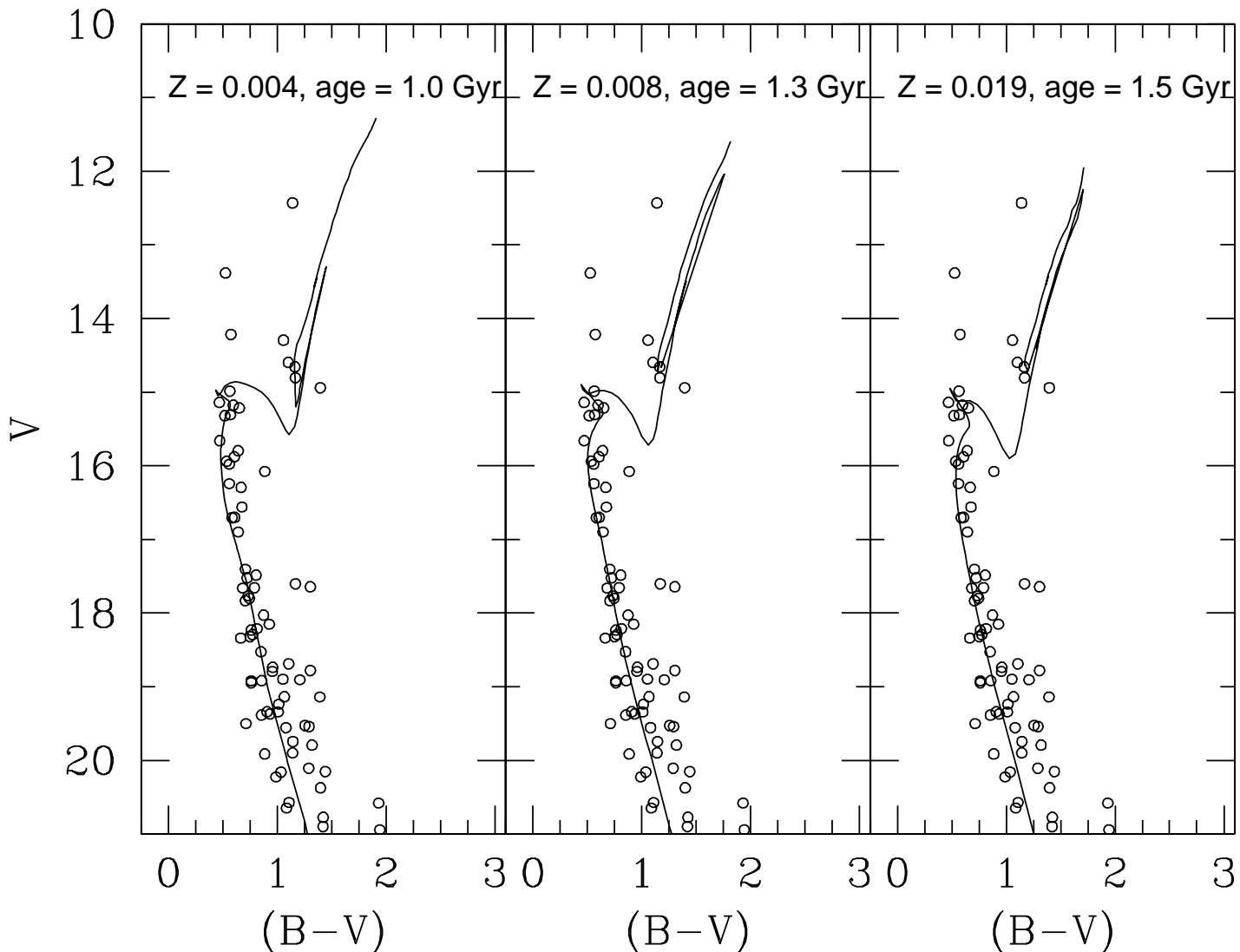


Figure 10. Hunting for the best fit isochrone solution. The CMD of Ruprecht 61 is shown together with three different isochrones. The isochrones are for the age of 1 Gyr and metallicity $Z=0.004$ in the left panel, for the age of 1.3 Gyrs and metallicity $Z=0.008$ in the middle panel, and, finally, for the age of 1.5 Gyrs and metallicity $Z=0.019$ in the right panel.

Galactocentric distance of 9.4 kpc, assuming 8.5 kpc as the distance of the Sun to the Galactic Center.

Czernik 32. The isochrone solution for this cluster is displayed in Fig.12. We obtained the best fit for an age of 1 Gyr and a metallicity $Z=0.008$. The inferred reddening and apparent distance modulus are $E(B-V)=0.85$ ($E(V-I)=1.08$) and $(m-M)=15.7$, respectively. These values situate the cluster at a heliocentric distance of 4.1 kpc, which corresponds to a Galactocentric distance of 10.8 kpc. The overall fit is also good in this case, the detailed shape of the MS and TO are nicely reproduced, as well as the color of the clump.

NGC 2225. The isochrone solution for this cluster is presented in Fig.13. We obtained the best fit for an age of 1 Gyr and a metallicity $Z=0.008$, which reproduces the sharp

cluster sequence extremely well. The inferred reddening and apparent distance modulus are $E(B-V)=0.35$ ($E(V-I)=0.50$) and $(m-M)=13.6$, respectively. Therefore the cluster has a heliocentric distance of 3.2 kpc, and is located at a Galactocentric distance of 11.2 kpc.

NGC 2262. The isochrone solution for this cluster is shown in Fig.14. We obtained the best fit for an age of 1 Gyr and a metallicity of $Z=0.008$. The inferred reddening and apparent distance modulus are $E(B-V)=0.55$ ($E(V-I)=0.72$) and $(m-M)=14.5$, respectively, which put the cluster at a heliocentric distance of 3.6 kpc, or at a Galactocentric distance of 11.7 kpc.

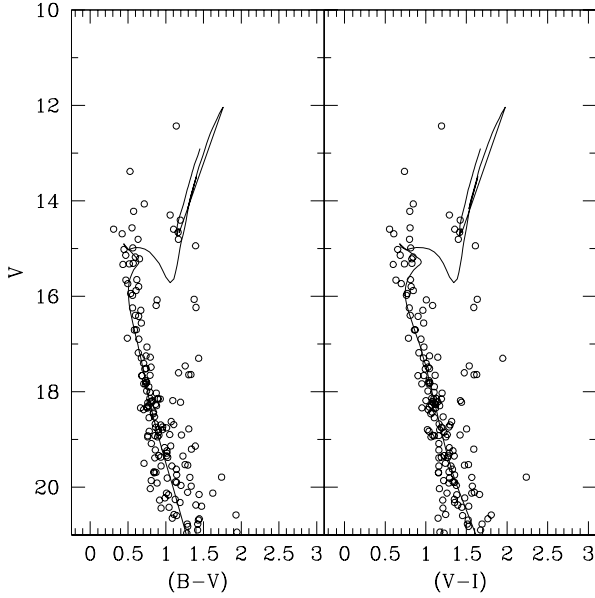


Figure 11. Isochrone solution for Ruprecht 61. The isochrone is for the age of 1.3 Gyr and metallicity $Z=0.008$. The apparent distance modulus is $(m-M)=13.85$, and the reddening $E(B-V)=0.30$ and $E(V-I)=0.41$. See text for more details. Only stars within the derived radius are shown.

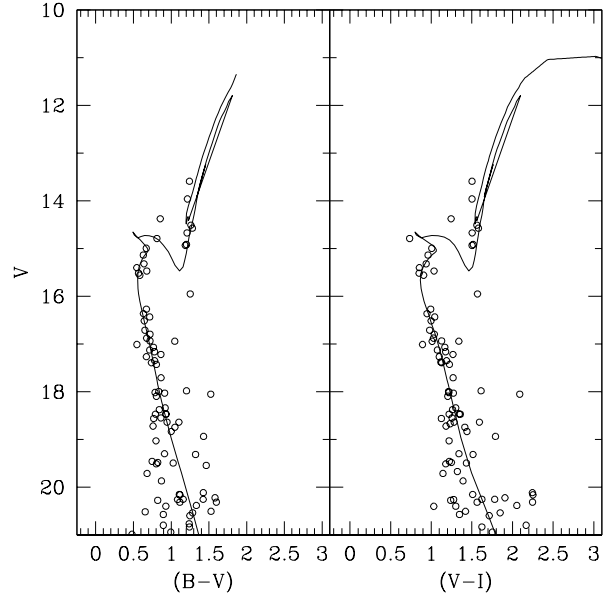


Figure 13. Isochrone solution for NGC 2225. The isochrone is for the age of 1.3 Gyrs and metallicity $Z=0.008$. The apparent distance modulus is $(m-M)=13.5$, and the reddening $E(B-V)=0.35$ and $E(V-I)=0.56$. See text for more details. Only stars within the derived radius are shown.

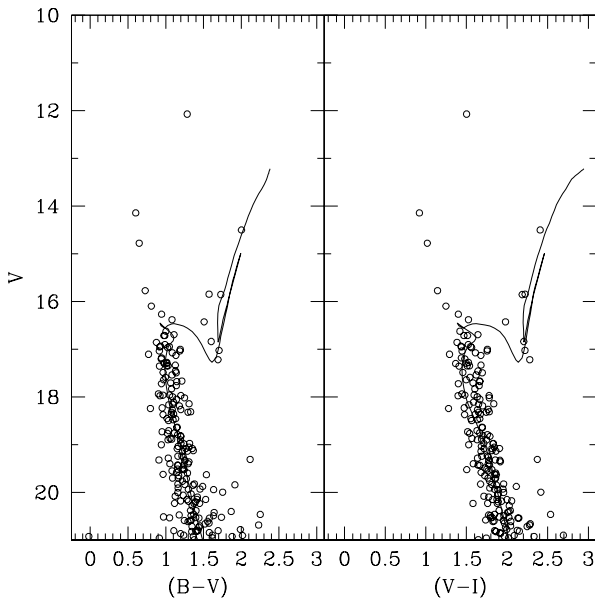


Figure 12. Isochrone solution for Czernik 32. The isochrone is for the age of 1 Gyr and metallicity $Z=0.008$. The apparent distance modulus is $(m-M)=15.7$, and the reddening $E(B-V)=0.85$ and $E(V-I)=1.08$. See text for more details. Only stars within the derived radius are shown.

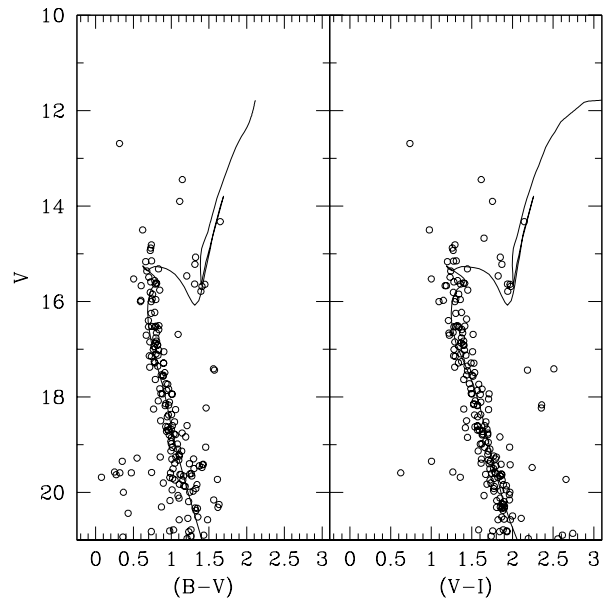


Figure 14. Isochrone solution for Czernik 32. The isochrone is for the age of 1 Gyr and metallicity $Z=0.008$. The apparent distance modulus is $(m-M)=14.5$, and the reddening $E(B-V)=0.55$ and $E(V-I)=0.72$. See text for more details. Only stars within the derived radius are shown.

6 CONCLUSIONS

We have presented the first CCD *BVI* photometric study of the star clusters Ruprecht 61, Czernik 32, NGC 2225 and NGC 2262. Through a star count analysis we have refined previous estimates of the clusters' coordinates and apparent radii. A detailed comparison of the clusters' CMDs with theoretical isochrones has allowed us to infer the aggregates' basic parameters and their uncertainties, which are summarized in Table 4.

In detail, the fundamental findings of this paper are:

- the best fit reddening estimates support within the errors a normal extinction law toward the four clusters;
- all the clusters turn out to be of intermediate age, and not far from the Sun toward the anti-center direction.
- the photometric estimates of the metallicity are lower than solar, as expected for clusters located between 9 and 11 kpc from the Galactic Center (Carraro et al. 1998).

ACKNOWLEDGEMENTS

The observations presented in this paper have been carried out at Cerro Tololo Interamerican Observatory CTIO (Chile). CTIO is operated by the Association of Universities for Research in Astronomy, Inc. (AURA), under a cooperative agreement with the National Science Foundation as part of the National Optical Astronomy Observatory (NOAO). The work of G.C. is supported by *Fundación Andes*. D.G. gratefully acknowledges support from the Chilean *Centro de Astrofísica* FONDAF No. 15010003. This work has been also developed in the framework of the *Programa Científico-Tecnológico Argentino-Italiano SECYT-MAE Código: IT/PA03 - UIII/077 - período 2004-2005*. A.M. acknowledges support from FCT (Portugal) through grant SFRH/BPD/19105/2004. This study made use of Simbad and WEBDA databases.

REFERENCES

- Baume G., Moitinho A., Giorgi E., Carraro G., Vazquez R., 2004, *A&A* 417, 961
- Carraro G., Chiosi C., 1994, *A&A* 287, 761
- Carraro, G., Ng Y.K., Portinari L., 1998, *MNRAS*
- Carraro G., 2005, *ApJ* 621, L61
- Carraro G., Geisler D., Baume G., Vazquez R., & Moitinho A., 2005, *MNRAS* 360, 655
- Chiosi C., Bertelli G., Bressan A. 1992, *ARA&A* 30, 235
- Dias W.S., Alessi B.S., Moitinho A., Lepine J.R.D., 2002, *A&A* 389, 871
- Girardi L., Bressan A., Bertelli G., Chiosi C., 2000, *A&AS* 141, 371
- Landolt A.U., 1992, *AJ* 104, 340
- Lynga G., 1982, *A&A* 109, 213
- Moitinho A., 2001, *A&A* 370, 436
- Moitinho A., Carraro G., Baume G., Vazquez R., 2005, *A&A* submitted
- Patat F., Carraro G., 2001, *MNRAS* 325, 1591
- Stetson P.B. 1987, *PASP* 99, 191

Table 4. Fundamental parameters of the studied clusters. The coordinates system is centered on the Sun, with the X and Y axes lying on the Galactic plane and Z perpendicular to the plane. Y points in the direction of the Galactic rotation, being positive in the first and second Galactic quadrants; Y points toward the Galactic anticenter; and Z indicates the north Galactic pole (Lynga 1982).

<i>Name</i>	<i>Radius</i> ($'$)	<i>E(B - V)</i>	<i>E(V - I)</i>	<i>(m - M)</i>	<i>d</i> $_{\odot}$	<i>X(kpc)</i>	<i>Y(kpc)</i>	<i>Z(kpc)</i>	<i>R_{GC}(kpc)</i>	<i>Age(Gyr)</i>	<i>Metallicity</i>
Ruprecht 61	1.0	0.30±0.1	0.41±0.1	13.85±0.2	3.9	-3.8	1.1	0.19	9.4	1.3±0.2	0.008±0.002
Czernik 32	1.0	0.85±0.1	1.08±0.1	15.70±0.2	4.1	-1.7	3.7	-0.12	10.8	1.0±0.3	0.008±0.002
NGC 2225	1.2	0.35±0.1	0.50±0.1	13.60±0.2	3.2	-1.9	2.5	-0.55	11.2	1.3±0.2	0.008±0.003
NGC 2262	1.0	0.55±0.1	0.72±0.1	14.50±0.2	3.6	-1.8	3.1	-0.13	11.7	1.0±0.2	0.008±0.004